Analytical models of calcium binding in a calcium channel

Jinn-Liang Liu and Bob Eisenberg

Citation: The Journal of Chemical Physics **141**, 075102 (2014); doi: 10.1063/1.4892839
View online: http://dx.doi.org/10.1063/1.4892839
View Table of Contents: http://scitation.aip.org/content/aip/journal/jcp/141/7?ver=pdfcov
Published by the AIP Publishing

Analytical models of calcium binding in a calcium channel

Jinn-Liang Liu[1] and Bob Eisenberg[2]
[1]*Department of Applied Mathematics, National Hsinchu University of Education, Hsinchu 300, Taiwan*
[2]*Department of Molecular Biophysics and Physiology, Rush University, Chicago, Illinois 60612, USA*

(Received 4 June 2014; accepted 30 July 2014; published online 19 August 2014)

The anomalous mole fraction effect of L-type calcium channels is analyzed using a Fermi like distribution with the experimental data of Almers and McCleskey [J. Physiol. **353**, 585 (1984)] and the atomic resolution model of Lipkind and Fozzard [Biochemistry **40**, 6786 (2001)] of the selectivity filter of the channel. Much of the analysis is algebraic, independent of differential equations. The Fermi distribution is derived from the configuration entropy of ions and water molecules with different sizes, different valences, and interstitial voids between particles. It allows us to calculate potentials and distances (between the binding ion and the oxygen ions of the glutamate side chains) directly from the experimental data using algebraic formulas. The spatial resolution of these results is comparable with those of molecular models, but of course the accuracy is no better than that implied by the experimental data. The glutamate side chains in our model are flexible enough to accommodate different types of binding ions in different bath conditions. The binding curves of Na^+ and Ca^{2+} for [$CaCl_2$] ranging from 10^{-8} to 10^{-2} M with a fixed 32 mM background [NaCl] are shown to agree with published Monte Carlo simulations. The Poisson-Fermi differential equation—that includes both steric and correlation effects—is then used to obtain the spatial profiles of energy, concentration, and dielectric coefficient from the solvent region to the filter. The energy profiles of ions are shown to depend sensitively on the steric energy that is not taken into account in the classical rate theory. We improve the rate theory by introducing a steric energy that lumps the effects of excluded volumes of all ions and water molecules and empty spaces between particles created by Lennard-Jones type and electrostatic forces. We show that the energy landscape varies significantly with bath concentrations. The energy landscape is not constant. © *2014 AIP Publishing LLC*. [http://dx.doi.org/10.1063/1.4892839]

I. INTRODUCTION

The "all-spheres" model of voltage-gated calcium (Ca_V) channels introduced by Nonner and Eisenberg[1–4] has stimulated many papers on primitive models of selectivity in biological channels (some 30 papers reviewed in Ref. 5; see more recent work cited in Refs. 6–16). Calcium selective channels[17,18] and electrochemical diodes[19] have actually been built, inspired by the model, as the critical role of the interactions of crowded protein side chains and permeating ions came to be understood.[20,21] The literature is described toward the end of the paper.

The all-spheres model has been analyzed in the literature with methods that use interatomic forces to enforce steric discipline and prevent overlap. Steric forces of this sort can be expensive to compute[6] and introduce certain mathematical difficulties because they are nearly singular.

A different way to prevent two ions from occupying the same space is to compute energies and forces from an adaptation of the Fermi distribution that automatically prevents overlap. Thomas and Fermi used this approach[22] early in the history of quantum mechanics (in place of the Pauli exclusion principle) to enforce Fermi-Dirac statistics for particles that do not overlap. A formal derivation of a Fermi like distribution of ions with different sizes and valences in general electrolyte solutions has been developed in Ref. 15 by deriving the configuration entropy of hard spheres. Important historical antecedents of steric effects are discussed in Refs. 23–25. Advances in numerical methods[25] allow three-dimensional calculations of calcium channels using the Poisson-Fermi differential equation with results quite similar to experiments and Monte Carlo simulations.[15,25]

A great deal of chemistry has been deduced from the equilibrium properties of statistical distributions without using the field theories found in most of physics. Differential equations are noticeable by their absence in classical textbooks of statistical mechanics[26] compared to those of multiparticle physics.[27] We imagine that using the Fermi distribution instead of the Boltzmann distribution in analysis of ions and water molecules in solutions and channels is likely to help deal with the nonideal properties of bulk solutions that arise from the finite volume of particles. Nonideal properties are particularly important in biology where divalents, concentrated bulk solutions, and mixtures are nearly always present.[12] The Fermi distribution provides a natural description of the saturation of concentration produced by the crowding of ions[5] near "working" electrodes of electrochemical cells, and in and near ion channels, nucleic acids, and active sites of enzymes.[28] Here, we emphasize the biological application but we are quite aware that the Fermi like distribution and the Poisson-Fermi equation imply a reasonably general "all spheres" theory of electrolyte solutions and mixtures.

We show that important binding properties of the calcium channel can be calculated by algebra alone using the Fermi like distribution that takes into account ions of any size and water molecules and satisfies the saturation condition of ionic concentrations in mean field theory. In a certain sense, the Fermi distribution allows analysis much as classical statistical mechanics allows analysis using the Boltzmann distribution. Neither needs differential equations or boundary conditions to describe many important (e.g., integral) properties of binding systems. Partial differential equations are needed to probe spatial profiles—and we use them here—and will be needed to explore time dependence and dissipation.[6,11,29–31]

This paper is organized with an introduction to the all-spheres model and a general discussion of the Fermi approach to ions and water in solutions and channels in Sec. II. The anomalous mole fraction effect and the Lipkind-Fozzard molecular model are presented in Sec. II A. Section II B contains all algebraic formulas derived from the Fermi distribution and all numerical results of binding phenomena obtained directly from the experimental data and these formulas. The Poisson-Fermi differential equation[15,25] is given in Sec. II C and then used to look into the channel with more resolution. The energy and concentration profiles are outputs of both algebraic Fermi and Poisson-Fermi differential equations. They are shown in Sec. II C including the effects of a 10^6-fold variation of the Ca^{2+} bath concentrations. The variable profile of dielectric coefficient is another output of the Poisson-Fermi equation and is an important determinant of selectivity in DEKA sodium channels (Figs. 8–10 in Ref. 20)—closely related to L-type Ca_V channels. A literature survey to deal with the various treatments of the all-spheres model is given in Sec. III A Detailed structures of channels are being published every week. We outline an algebraic Fermi approach in Sec. III B to the structure of a calcium/sodium exchanger recently published by Liao *et al.*[32] We think it is more helpful to provide an outline to a specific problem than to discuss generalities. Some concluding remarks are given in Sec. IV.

II. MODEL AND RESULTS

A. Ca_V channel and mole fraction effect

A signature property of Ca_V channels is the anomalous mole fraction effect. Trace concentrations of Ca^{2+} ions effectively block the flow of abundant monovalent cations.[33–38] A variety of experimental results show that the EEEE locus (four glutamate side chains) is a high-affinity Ca^{2+} binding structure in the pore of Ca_V channels and is essential to Ca^{2+} selectivity and blockage.[39–49] Each glutamate has a terminal carboxylate COO^- group so the pore has a charge of $-4e$,[41] where e is the proton charge. The EEEE structure is quite flexible in simulations[50,51] and the glutamates are accessible to ions and reagents from the surrounding baths.[52–56] The glutamates mix with permeating ions[7,13,20,21] over a wide range of concentrations in the solutions surrounding the channel and so the selectivity filter is a mixture of Ca^{2+} and Na^+ ions and carboxylates COO^- from the glutamate side chains of the channel protein. Physiological Ca^{2+} levels vary from 10^{-8} M in resting cytoplasm, to 10^{-6} M in activated contractile tissue, to 10^{-3} M in typical extracellular solutions, to >1 M, probably >10 M, in and near ion channels, active sites of enzymes, binding proteins, and nucleic acids. The binding mechanism in the L-type Ca_V channel operates over a 10^8-fold range of experimental Ca^{2+} concentration[33] and so poses a serious challenge to all atom simulations as well as theoretical models.[57]

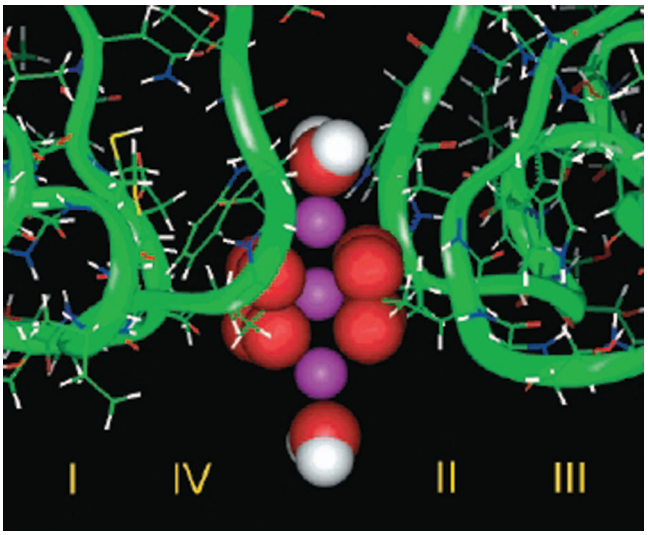

FIG. 1. The Lipkind-Fozzard pore model, where 3 Ca^{2+} are shown in violet, 8 $O^{1/2-}$ in red, 2 H_2O in white and red. Reprinted with permission from G. M. Lipkind and H. A. Fozzard, Biochemistry **40**, 6786 (2001). Copyright (2001) American Chemical Society.

We illustrate the use of the Fermi distribution with an analysis of a particular calcium selective structure proposed by Lipkind and Fozzard[50] and outline how the Fermi distribution can be applied to a real channel structure recently published.[32] Fig. 1 illustrates the binding site, the filter, and the EEEE locus, where 3 Ca^{2+} are shown in violet, 8 $O^{1/2-}$ in red, 2 H_2O in white and red. If a Ca^{2+} occupies the binding site, this molecular model shows that there is no room for other particles in the filter as the 8 oxygen ions are tightly attracted toward the Ca^{2+} ion. On the other hand, if a Na^+ is located at the site, the pore radius of the filter is enlarged by the strong repulsion of the oxygen ions making sufficient room for other particles. The EEEE binding site can be filled by two calcium ions or four sodium ions. The volume of the extra two sodium ions produces a substantial energy penalty that is an important determinant of selectivity in this calcium channel. Fig. 2 is a cross section of a simplified three-dimensional channel geometry of Fig. 1. The solvent region Ω_s consists of two baths and the channel pore including the filter region.

The flexibility of the EEEE (Glu–Glu–Glu–Glu) structure and the binding mechanism[3] are analyzed by the Fermi distribution function using the experimental result of Almers and McCleskey[33] that the Na^+ current is halved in a L-type calcium channel at the "midpoint of the binding curve" (see below), namely, when

$$\underbrace{C^{\mathrm{B}}_{\mathrm{Na}^+} = C^{\mathrm{B}}_1 = 32\ \mathrm{mM},\ C^{\mathrm{B}}_{\mathrm{Ca}^{2+}} = C^{\mathrm{B}}_2 = 0.9\ \mu\mathrm{M}}_{\text{Experimental Data}}, \qquad (1)$$

where $C^{\mathrm{B}}_{\mathrm{Na}^+}$ and $C^{\mathrm{B}}_{\mathrm{Ca}^{2+}}$ are the (bulk) concentrations of the salts NaCl and $CaCl_2$ in baths, respectively. A trace

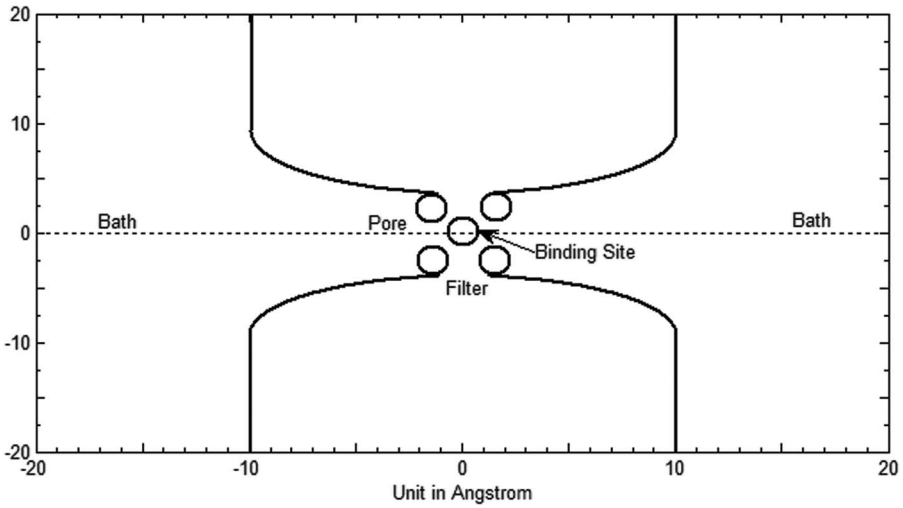

FIG. 2. A simplified Ca channel geometry with baths, pore, filter, and binding site. The channel is placed in a cubic box with the length of each side being 40 Å.

concentration of calcium [Ca^{2+}], 36,000× smaller than the concentration of sodium ion [Na^+], is enough to bring the channel to the midpoint of the binding curve. The channel has a binding selectivity 36,000× higher for Ca^{2+} than Na^+ ions. The particle species are indexed by 1, 2, 3, and 4 for Na^+, Ca^{2+}, Cl^-, and H_2O with radii $a_1 = a_{Na^+} = 0.95$, $a_2 = a_{Ca^{2+}} = 0.99$, $a_3 = a_{Cl^-} = 1.81$, and $a_4 = a_{H_2O} = 1.4$ Å, respectively.

B. Algebraic Fermi model

There is more than one way to introduce the Fermi distribution and none is as well determined as a full field theory model of an ion channel, using the Poisson-Fermi differential equation[15] or other field theories and models.[6,11,29,30] We use a simple approach to explore what can be done with algebra alone. We are motivated by curiosity and also by the realistic knowledge that thousands of experimental biologists studying channels everyday are far more likely to use an approach that depends on algebra than one that depends on differential equations, let alone variational theory. Our goal is to develop methods that experimental scientists can use to analyze the data they measure everyday without depending on theoretical methods and colleagues they have difficulty evaluating or understanding. Since a great deal of useful chemistry has been done using algebraic properties of statistical distributions, before ordinary or partial differential equations could be actually solved, we have some hope of success.

Our first question is the following. Can we find an analytical—not simulation—method that can directly connect the bath condition Eq. (1) to the properties (e.g., concentration or location) of binding ions? We avoid all atom simulations because of the difficulties they have in dealing with the biological range of calcium concentrations. Biological concentrations of Ca^{2+} are often 10^{-8}-10^{-6} M and all atom simulations are not yet large enough to deal with the 55 M water that dissolves each calcium ion in a 10^{-8}-10^{-6} M Ca^{2+} solution.[57] The experimental properties we choose as our starting point (the midpoint of a binding curve (1)) are of the type used by experimental biophysicists and biochemists for generations to characterize binding.

At first glance, it seems unlikely that experimental data concerning macroscopic concentrations could be used to determine atomic scale properties in the channel. After all, the binding ion is millions of Angstroms away from the location where these bath concentrations are measured. But the combination of the all-spheres model and the Fermi distribution does in fact allow one to determine some atomic properties of the binding site, as we shall see.

The potential function $\phi(\mathbf{r})$ for ions in or near a channel provides a tool to establish such a connection, where $\mathbf{r}$ is a space variable. By including specifically the excluded volume effect of water molecules and interstitial voids between all particles, we extend the Fermi like distribution of Ref. 15 to

$$C_i(\mathbf{r}) = C_i^{\mathrm{B}} \exp(-\beta_i \phi(\mathbf{r}) + S^{\mathrm{trc}}(\mathbf{r})) \tag{2}$$

that describes the concentration of particles of type i in an electrolyte solution with arbitrary K species of ions and the last species $(K+1)$ of water molecules at any location $\mathbf{r}$ in the solvent domain Ω_s. The concentration function is determined by the bulk concentration C_i^{B} (constant), the electrostatic potential $\phi(\mathbf{r})$, and the "steric" potential

$$S^{\mathrm{trc}}(\mathbf{r}) = \ln \frac{1 - \sum_{j=1}^{K+1} v_j C_j(\mathbf{r})}{1 - \sum_{j=1}^{K+1} v_j C_j^{\mathrm{B}}} \tag{3}$$

that in turn depends on all concentration functions $C_j(\mathbf{r})$. Here, $\beta_i = q_i/(k_B T)$, $q_i = z_i e$, z_i is the valence of the particle, k_B is the Boltzmann constant, T is the absolute temperature, and $v_i = 4\pi a_i^3/3$ is the volume of the particle with radius a_i. Note $q_{K+1} = \beta_{K+1} = 0$ and the steric potential is a scalar function that corresponds to a steric force field just as the electric potential ϕ corresponds to the electric force field. The empty space (void) between particles is expressed by the void fraction function $\Gamma(\mathbf{r}) = 1 - \sum_{j=1}^{K+1} v_j C_j(\mathbf{r})$.

The Fermi distribution function is derived from the configuration entropy of hard-sphere ions and water and can be shown[15] to satisfy the saturation condition $C_j(\mathbf{r}) \le 1/v_j$ for

all different sizes of particles, for all points $\mathbf{r}$ in the domain, even at infinitely large potential $\phi(\mathbf{r})$. The steric potential (3) approximates the effects of Lennard-Jones potentials between all pairs of particles in a mean-field sense. The zero steric potential $S^{\text{trc}}(\mathbf{r}) = 0$ corresponds to the zero Lennard-Jones potential of all particles at the bulk condition, which yields the constant void fraction $\Gamma^{\text{B}} = 1 - \sum_{j=1}^{K+1} v_j C_j^{\text{B}}$. The classical Boltzmann distribution appears if all particles are treated as volumeless points, i.e., $v_i = 0$. Then, an infinite concentration occurs in some crowded conditions—e.g., close to charged surfaces—an impossible result. This result represents an unbounded flaw in the classical Boltzmann approach when applied to ionic solutions in crowded conditions. It should be emphasized that ionic solutions are often crowded where they are most important, near working electrodes, and in and near ionic channels, binding proteins, enzyme active sites, and nucleic acids. The unbounded flaw is documented in a large literature[5,15,23–25,58–60] even though the flaw has not yet spread into the textbook literature, as far as we know, or into the general knowledge of many biologists[12] or mathematicians.[61]

Following classical statistical mechanics,[26] we use the Fermi distribution (2) to link the probabilistic quantities of ions in the binding site to concentrations C_i^{B} in the baths, i.e.,

$$\begin{cases} P_1 = v_b C_1^{\text{B}} \exp(-\beta_1 \phi_A + S^{\text{trc}}) \\ P_2 = v_b C_2^{\text{B}} \exp(-\beta_2 \phi_A + S^{\text{trc}}) \end{cases}, \tag{4}$$

where P_1 and P_2 are given, v_b is an unknown variable volume (due to the unknown void volume enclosing the ion) of the binding site, ϕ_A is an average potential in the binding site, and A is any point on the surface of the site. P_1 means that a Na^+ can be found in v_b with the probability of P_1 when the ion possesses an energy $(-\beta_1 \phi_A + S^{\text{trc}}) k_B T = -\mathcal{E}_1$ under a given bath condition C_1^{B} and C_2^{B}, where $\mathcal{E}_1$ is a state energy, for example, the energy well in Ref. 62. By (3), the steric potential in the binding site

$$S^{\text{trc}} = \ln \frac{v_b - v_1 P_1 - v_2 P_2}{v_b \Gamma^{\text{B}}} \tag{5}$$

establishes a relation between S^{trc} and v_b. Note that the energy well $\mathcal{E}_1$ consists of not only the electrostatic energy $\beta_1 \phi_A k_B T$ but also the steric energy $-S^{\text{trc}} k_B T$. The steric energy is related to the vacancy diffusion mechanism[63] that results from the fluctuations of protein side chains caused by thermal agitation and polarization forces from the binding ion. The steric energy was not included in the classical rate theory used to study ion channel selectivity and permeation.[62,63] The changes in structure and steric energy that occur when ion composition or concentrations are changed in the baths are also not included in classical rate theories, with unfortunate consequences.[2,7]

The properties of binding sites in channels are typically summarized by the conditions necessary to produce half block[63] following the age old practice of enzymologists.[65] For the half-blockage experimental condition $C_1^{\text{B}} = 32$ mM and $C_2^{\text{B}} = 0.9$ μM, we follow convention and assume relative occupancies of a filled channel, $P_1 = 0.5$ and $P_2 = 0.5$, and thereby obtain $\phi_A = -10.478\ k_B T/e$, $S^{\text{trc}} = -1.8$, and $v_b = 4.3$ Å^3. The value $S^{\text{trc}} = -1.8$ is dimensionless leading to the water density $C_4 = C_4^{\text{B}} \exp(-1.8) = 5$ M with $C_4^{\text{B}} = 55.5$ M and the probability $P_4 = 0.06$ in the binding site.

The void fraction in the binding site is $\Gamma = 0.04$ indicating that a small volume of empty space surrounds the binding ion in mean-field sense. It is important to include the void volume both to make our treatment fully consistent and to deal with the possibility that the void volume might vary with conditions. Remember the volume is an output of models like these.[3] These results were obtained by Eqs. (4) and (5) with the binding volume v_b. From Fig. 1, the filter region is larger than the binding volume. Fig. 3 is a simplified 2D sketch of a cylindrical filter with radius of the binding site and length $L = 4.47$ Å, which contains the binding site. We investigate the half blockage conditions in the whole filter (not just the binding site) by setting $\phi_A = -10.478\ k_B T/e$, $P_1 = 0.5$, and $P_2 = 0.5$ in the filter and changing the binding volume v_b to the filter volume v_f in (4). In that case, the steric energy is $S^{\text{trc}} = -3$ and the Na^+ and Ca^{2+} concentrations $C_1 = C_2 = 59$ M in the filter.

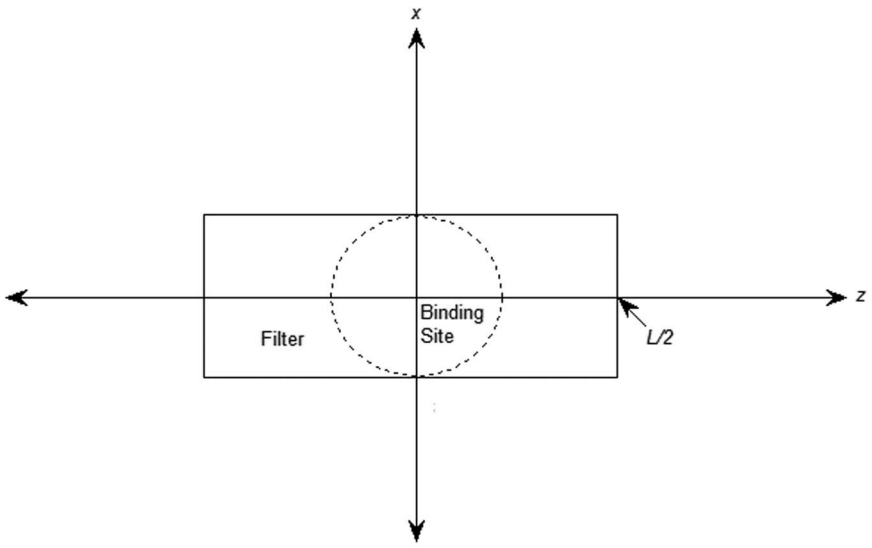

FIG. 3. Definition of the cylindrical filter contained in the solvent domain Ω_s with length L and radius of the binding site.

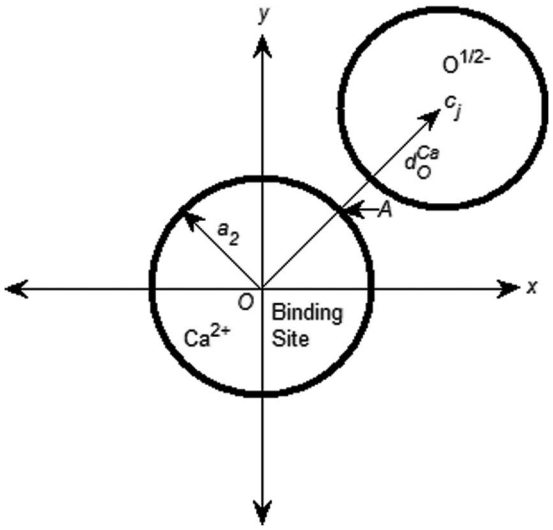

FIG. 4. A 2D sketch of the binding site with radius a_2 and a neighboring $O^{1/2-}$. The distance between the centers of the binding site and any $O^{1/2-}$ ion is denoted by D_O^{Ca}.

The selectivity filter is crowded. It is nearly filled by the large concentration of ions—59 M—but these do not overfill the space available. In this treatment using a Fermi like distribution, the filter does not suffer from the unbounded error found in treatments using the classical Boltzmann distribution. Both ionic species satisfy the saturation condition (e.g., $C_2 \le C_2^{\text{Max}} = \frac{1}{v_2} = 408.6$ M) while they embody the strong binding and selectivity that allow the real L-type calcium channel to function selectively in the heart.

The model and procedure used here allow estimation of the distance between the binding ion and structural oxygens (i.e., half charged oxygen atoms of the glutamate side chains) of the all-spheres model. If a Ca^{2+} is located at the binding site, the binding distance d_O^{Ca} between any pair of Ca^{2+} and $O^{1/2-}$ is estimated by the binding formula

$$\frac{e}{4\pi\epsilon_f\epsilon_0}\sum_{j=1}^{8}\left(\frac{z_{O^{1/2-}}}{|c_j - A|} + \frac{P_1 z_{Na^+}}{a_{Na^+}} + \frac{P_2 z_{Ca^{2+}}}{a_{Ca^{2+}}}\right) = \phi_A, \quad (6)$$

with $P_1 = 0$, $P_2 = 1$, and $\phi_A = -10.478$, where ϵ_0 is the vacuum permittivity, ϵ_f is a dielectric constant in the filter that is called the relative permittivity in physical chemistry,[64] $z_{O^{1/2-}} = -1/2$, $z_{Ca^{2+}} = 2$, and $|c_j - A|$ is the distance between A and the center of the jth $O^{1/2-}$ as shown in Fig. 4. The distance $|c_j - A|$ depends only on d_O^{Ca} which is unknown and unique due to symmetry.

Solving (6) exactly with $\epsilon_f = 1$ yields $d_O^{Ca} = 2.24$ Å. Again, this number is only as precise as the experimental data cited in (1) and so estimates of distances directly reflect uncertainties in measurement, as well as uncertainties in our theory. We present these results to show that the model and method easily allow the determination of locations. We do not believe that these are the actual locations of ions, because we do not have evidence that the Lipkind-Fozzard model describes a real channel. It is striking to us that the Fermi distribution allows us to map macroscopic binding data directly into spacing of binding sites in the all-spheres model using minimal structural information. When the binding site is occupied by a Na^+, i.e., $P_1 = 1$ and $P_2 = 0$, the binding distance changes name to d_O^{Na} and we get $d_O^{Na} = 4.527$ Å. The location of $O^{1/2-}$ is very different from that when calcium occupies the filter. The charge (valence) difference between Ca^{2+} and Na^+ dramatically changes the binding distance from $d_O^{Na} = 4.527$ Å to $d_O^{Ca} = 2.24$ Å (remember that the diameter of calcium and sodium are nearly the same). This change in distance goes along with and is, in some sense, the cause of (part of) the 36,000-fold selectivity of the filter and the steric effect.

This change in structure reflects the flexibility of four glutamate side chains that allows and reflects a change of pore radius of about 2.3 Å. Our figure of 2.3 Å is surprisingly (and gratifyingly) close to the value of 2 Å found by Barreiro *et al.*[51] using molecular dynamics simulations. We identify the radius of $O^{1/2-}$ as the covalent radius $a_{O^{1/2-}} = 0.7$ Å so that the distance $d_O^{Ca} = 2.24$ Å is slightly larger than $a_{Ca^{2+}} + a_{O^{1/2-}} = 1.69$ Å (see Fig. 4). The effects of changes in structure with concentrations in the bath were considered as soon as the all-spheres model was introduced.[3]

We choose the filter dielectric constant $\epsilon_f = 1$ for this simple molecular model. For a real protein structure, the chelating ions and molecules forming the binding site are charged and move in response to changes in the (local) electric field. They are polarization charges. Moreover, the number of charged atoms in and around the selectivity filter of the real protein is certainly more than eight. These charges all interact. That is to say, the movement of any one charge is changed by the charges and movement of the other charges. Thus, it is difficult if not impossible to compute the polarization and the (effective) dielectric response in this model, starting with a real structure. Rather, we must choose a value of the effective dielectric constant and view it as a measure of the (effective, more or less) "Born solvation energy" needed to move a permeating or binding ion from the bulk to the binding site. Consequently, the filter dielectric constant in this mean-field model can only be chosen empirically to reflect the Born solvation energy.

The binding experiments[33] used a fixed $C^{\text{B}}_{Na^+} = C^{\text{B}}_1 = 32$ mM and various Ca^{2+} bath concentrations $C^{\text{B}}_{Ca^{2+}} = C^{\text{B}}_2$ that imply different probabilities P_1 and P_2 of Na^+ or Ca^{2+} occupying the filter. The probabilities P_1 and P_2 are determined by the following equation:

$$\frac{P_1}{P_2} = \frac{1 - P_2}{P_2} = \exp(\phi_A)\frac{C^{\text{B}}_1}{C^{\text{B}}_2}, \quad (7)$$

where $\phi_A = -10.478$ was obtained from the case of equal probability. The probability ratio thus deviates from unity as $C^{\text{B}}_{Ca^{2+}}$ is varied along the horizontal axis of the binding curve from its midpoint value $C^{\text{B}}_{Ca^{2+}} = 0.9$ μM as shown in Fig. 5, where the concentration of $CaCl_2$ is changed from 10^{-8} to 10^{-2} M while the concentration of NaCl is maintained at 32 mM in the baths. This figure clearly indicates that the probability of finding a Ca^{2+} in the filter is nearly zero when $[CaCl_2] = 10^{-8}$ M, the value in the cytoplasm of relaxed muscle which is not activated for contraction. At $[CaCl_2] = 10^{-5}$ M, the probability of finding a calcium ion in the filter dramatically increases to 0.85. The probability computed by

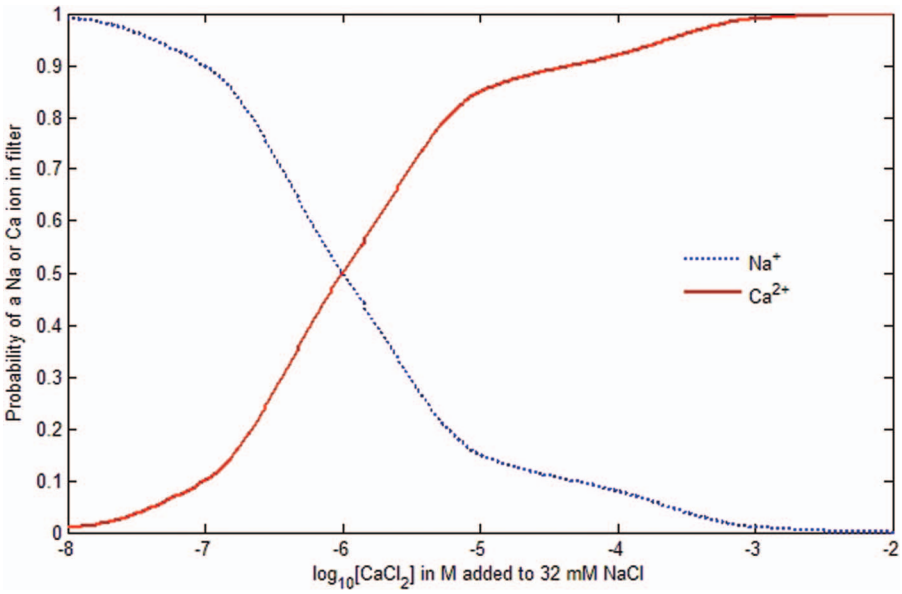

FIG. 5. Binding curves. The Na^+ and Ca^{2+} binding curves are comparable with Monte Carlo results[21] and show the probability change of a Na^+ or Ca^{2+} ion in the filter as the concentration of $CaCl_2$ from 10^{-8} M to 10^{-2} M is added to the fixed [NaCl] = 32 mM in the baths.

the Monte Carlo method[21] is 0.84 (estimated from Fig. 6(c) in Ref. 21). The probability of 0.5 for $[CaCl_2] = 0.9\ \mu$M also agrees with that of Monte Carlo simulations.

Note that the binding curves are obtained by fixing ϕ_A in Eqs. (6) and (7) as C_2^{B} is varied. Moreover, the flexibility of glutamate side chains with varying C_2^{B} is also deduced from this fixed ϕ_A. From Eq. (4), we observe that all P_1, P_2, v_b, and S^{trc} and other physical properties derived from these variables change with varying C_2^{B}. In effect, the changes of protein locations, binding probabilities, binding volume, binding energies, and others are all lumped into the changing steric energy S^{trc} via Eqs. (4) and (5) while the electrostatic potential ϕ_A is fixed in the binding site. Keeping ϕ_A fixed is equivalent to assuming that the relation (7) between the probability and bath concentration ratios is linear. More accurate models than this linear model may be needed if it fails to give accurate results for other physical properties or other systems.

It is important to note that the total energy of each ion also changes with varying C_2^{B} since the steric energy changes. The fixed electrical potential corresponds to the dissociation constant of a Ca^{2+} "bound" in an energy well in classical rate theory.[62] In a certain sense, our approach replaces the fixed electrical potential of rate theory with the variable steric potential of a consistent Fermi based theory. As mentioned in Ref. 62, the main limitation of the rate theory is that it does not invoke any physical distances, shape of pores, or location of atoms of protein structures, let alone varying bath conditions.

Our Fermi analysis improves the rate theory by showing that (i) Ca^{2+} energy wells $\mathcal{E}_2 = (\beta_2\phi_A - S^{\mathrm{trc}})k_BT$ vary with bath concentrations $C^{\mathrm{B}}_{\mathrm{Na}^+}$ and $C^{\mathrm{B}}_{\mathrm{Ca}^{2+}}$ (via S^{trc} in Eqs. (4) and (5)); energy wells are not constant; (ii) the protein structure (Eq. (6)) is an "evolutionary" consequence of a required potential energy ϕ_A to bind a Ca^{2+} in a site under certain physiological conditions on $C^{\mathrm{B}}_{\mathrm{Ca}^{2+}}$ and others; and (iii) the steric energy S^{trc} is used to lump the steric effects of excluded volumes of all ions and water molecules (Eq. (3)) and empty spaces between particles created by Lennard-Jones type (the void fraction function $\Gamma(\mathbf{r})$) and electrostatic forces (Eq. (6)).

C. Poisson-Fermi model

All numerical results obtained so far by algebra alone agree with those of published molecular models[50,51] or Monte Carlo analysis.[21] The next question is how to extend the potential function from the filter to the bath—from a single ion to numerous particles.

It is impractical (and unwise[57]) to treat all ions explicitly in the bath because they are numerous and their crowding effect is much less intense than that in the filter region. In the bulk solvent region, we compute the potential function $\phi(\mathbf{r})$ by solving the Poisson-Fermi equation[15,25,66,67]

$$\epsilon_s\left(l_c^2\nabla^2 - 1\right)\nabla^2\phi(\mathbf{r}) = \sum_{i=1}^{K+1} q_i C_i(\mathbf{r}) = \rho(\mathbf{r}) \tag{8}$$

together with Eqs. (2) and (3), where l_c is a correlation length,[66,67] $\epsilon_s = \epsilon_{\mathrm{w}}\epsilon_0$ in the bath or $\epsilon_f\epsilon_0$ in the filter, $\epsilon_{\mathrm{w}} = 78.5$ is the relative permittivity of water, and ρ is the charge density. The fourth-order Poisson-Fermi equation reduces to the classical Poisson-Boltzmann equation when $l_c = S^{\mathrm{trc}}(\mathbf{r}) = 0$. If $l_c \neq 0$, the dielectric operator $\widehat{\epsilon} = \epsilon_s(1 - l_c^2\nabla^2)$ approximates the permittivity of the bulk solvent and the linear response of correlated ions.[67] The dielectric function $\widetilde{\epsilon}(\mathbf{r}) = \epsilon_s/(1 + \eta/\rho)$ is a further approximation of $\widehat{\epsilon}$ and is found by transforming (8) to two second-order equations

$$\begin{cases} \epsilon_s\left(l_c^2\nabla^2 - 1\right)\Psi(\mathbf{r}) = \rho(\mathbf{r}) \\ \nabla^2\phi(\mathbf{r}) = \Psi(\mathbf{r}) \end{cases} \tag{9}$$

and introducing a density like variable Ψ that yields a polarization charge density $\eta = -\epsilon_s\Psi - \rho$ using Maxwell's first equation.[15,25] The binding potential ϕ_A is used as a Dirichlet

type condition for the potential function $\phi(\mathbf{r})$ in the filter domain while $\phi(\mathbf{r}) = 0$ on the extracellular and intracellular sides of the boundary and $\nabla\phi(\mathbf{r}) \cdot \mathbf{n} = 0$ on the other sides and on the remaining solvent boundary $\partial\Omega_s$, where $\mathbf{n}$ is an outward unit vector. An iterative process of solving equations in (9) and evaluating (2) and (3) is repeated until self-consistent $\phi(\mathbf{r})$ and $C_i(\mathbf{r})$ are reached within a tolerable error bound.[25]

The electrostatic potential $\phi(\mathbf{r})$ depends on all species of ions in (8) (via the concentration functions $C_i(\mathbf{r})$) and the screening effect of water molecules (via the correlation length l_c and the fourth order differential operator $\nabla^2\nabla^2$). The concentration functions $C_i(\mathbf{r})$ in turn computes the steric potential $S^{\text{trc}}(\mathbf{r})$ via (3) that includes all sizes and valences of ions and water. The concentration functions $C_i(\mathbf{r})$ are then re-evaluated via (2) for solving (9) in the next iteration. "Everything" interacts with everything else in crowded systems like this. Interactions are produced by crowding of the ions themselves, water molecules, and side chains of the protein, as well as by allosteric properties and conformation of the surrounding protein.

We do not need to solve the Poisson equation in the protein region that contains the singular charges of 8 $O^{1/2-}$ since the effect of these charges on potentials has been included in Eq. (6). Analysis is simplified significantly from our previous work.[25] We do not have to deal with the delta functions; we do not have any potential jump conditions on the interface (a molecular surface) between the bulk solvent and molecular regions. The absence of jump conditions facilitates a more accurate approximation of (9) by, for instance, the finite difference method because numerical methods for handling the jump conditions across molecular surfaces with cusps or with a singular Poisson equation are subtle, complex, and thus prone to error.[25,68]

Figs. 6–9 are the profiles of Na^+ concentration $C_1(\mathbf{r})$, Ca^{2+} concentration $C_2(\mathbf{r})$, Ca^{2+} energy well $\mathcal{E}_2(\mathbf{r}) = (\beta_2\phi(\mathbf{r}) - S^{\text{trc}}(\mathbf{r}))k_BT$, and dielectric function $\widetilde{\epsilon}(\mathbf{r})$, respectively, obtained by (9) using numerical methods developed in Ref. 25 for various Ca^{2+} bath conditions ranging from 10^{-7} to 10^{-2} M and the fixed $C^{\text{B}}_{\text{Na}^+} = C^{\text{B}}_1 = 32$ mM. Note that the most sensitive range is 10^{-7}-10^{-5} M, where Na^+ and Ca^{2+} probabilities vary steeply as shown in Fig. 5 so as $C_1(\mathbf{r})$ and $C_2(\mathbf{r})$ profiles shown in Figs. 6 and 7. From Fig. 8, we observe that Ca^{2+} energy wells change rapidly in the range 10^{-6}-10^{-2} M, where the depth of the energy well is significantly decreased by increasing Ca^{2+} ions and the conductance of the channel changes dramatically from allowing Na^+ to flow, to blocking Ca^{2+}, and then to allowing Ca^{2+} to flow as shown in the experiments (Fig. 11 in Ref. 33). The change of Ca^{2+} energy wells with varying C^{B}_2 is due mainly to the change of the steric potential $S^{\text{trc}}k_BT$, which is equivalent to the change of the binding distance from d_O^{Na} to d_O^{Ca} in Eq. (6). In the filter region, the steric potential $S^{\text{trc}}k_BT = -2.4, -3, -4.8, -7, -9.3$, and $-11.6\,k_BT$ for $C^{\text{B}}_{\text{Ca}^{2+}} = 10^{-7}, 10^{-6}, 10^{-5}, 10^{-4}, 10^{-3}$, and 10^{-2} M, respectively. Although the electrostatic and steric potentials are intimately connected to each other and to the bath condition via Eqs. (4) and (6), our analysis shows that channel selectivity and permeation are in fact critically determined by the steric effect that is not included in the classical rate theory of energy profiles.[62,63]

The theoretical selectivity of Ca^{2+} ions in the L-type calcium channel is very sensitive to bath concentrations of Ca^{2+} in the micro-molar range, just as is seen experimentally in Ref. 33. The signature phenomenon of L-type calcium channels emerges naturally from the Poisson-Fermi analysis of the all-spheres model. Trace concentrations of Ca^{2+} ions produce a sensitive midpoint block even in the presence of 36,000× more Na^+ ions.

The dielectric coefficient $\widetilde{\epsilon}(\mathbf{r})$ is found to vary from $\epsilon_w = 78.5$ in the baths to $\epsilon_f = 2$ in the filter as shown in Fig. 9. This variation of is a by-product—an output—of the Fermi distribution analysis (4) and the Poisson-Fermi differential

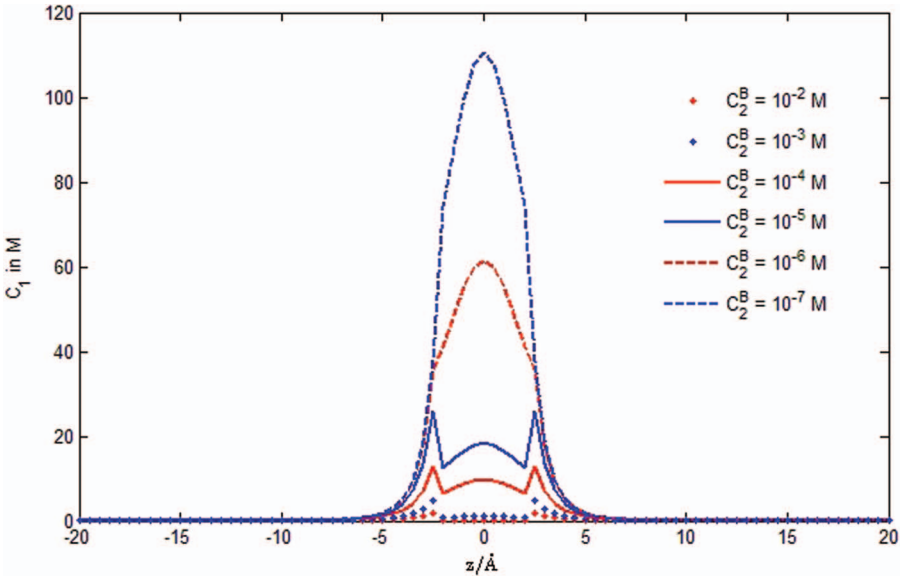

FIG. 6. The averaged concentration $C_1(\mathbf{r})$ profiles at each cross section along the pore axis for various C^{B}_2 ranging from 10^{-7} M to 10^{-2} M. All the following figures are obtained with the same averaging method and the same range of C^{B}_2.

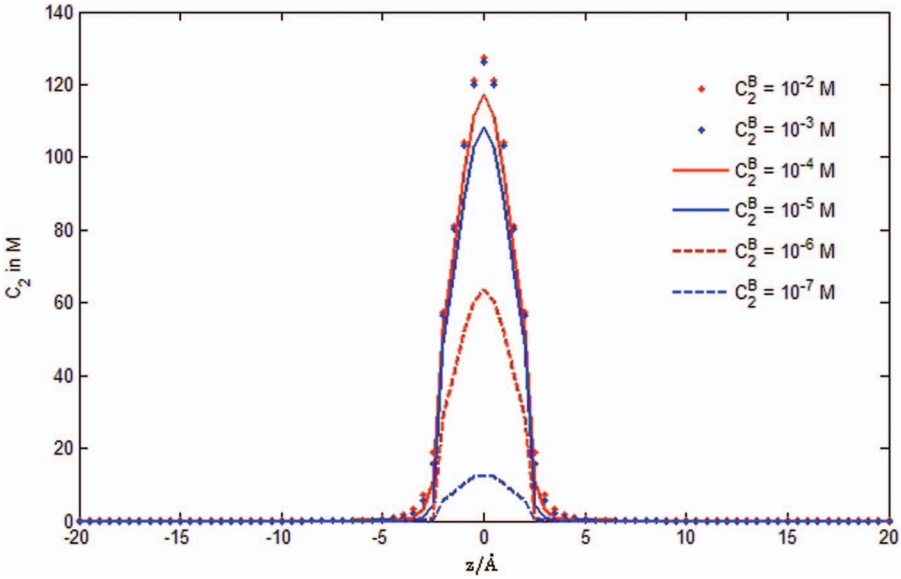

FIG. 7. The averaged concentration $C_2(\mathbf{r})$ profiles.

equation (8) when the correlation length is chosen to be $l_c = 2a_2 = 1.98$ Å.[67] We see that the polarization of water molecules depends essentially on the divergence of the electric field, i.e., on $\nabla \cdot \mathbf{E}(\mathbf{r}) = -\nabla \cdot \nabla\phi(\mathbf{r}) = -\Psi(\mathbf{r})$. By inspecting Figs. 8 and 9, we observe that the dielectric coefficient changes dramatically in the pore region near the filter (see Fig. 2), where the water molecules are strongly polarized by the large electric field.

III. DISCUSSION

A. Discussion of literature

The literature on the all-spheres model is large enough to be confusing so a discussion seems appropriate and hopefully helpful.

The all-spheres model has been mostly analyzed at equilibrium by Monte Carlo simulations, with the important exception of work on the RyR receptor by Gillespie and his co-workers.[37,69,70] They concatenated[69]—the density functional theory (DFT) of liquids[71]—and PNP equations—a useful nickname[72] for Poisson-Nernst-Planck,[73–76,83] emphasizing the analogy with the drift diffusion equations of semiconductors and PNP bipolar transistors—and found that the concatenation describes the ryanodine RyR channel very well.[70] They use an all-spheres model of the RyR and are able to predict detailed experimental results before the measurements were made. (It is important to consult the supplementary material of Ref. 70.)

Unfortunately, DFT-PNP does not naturally encompass the classical theory[77–79] of conductance of bulk solutions

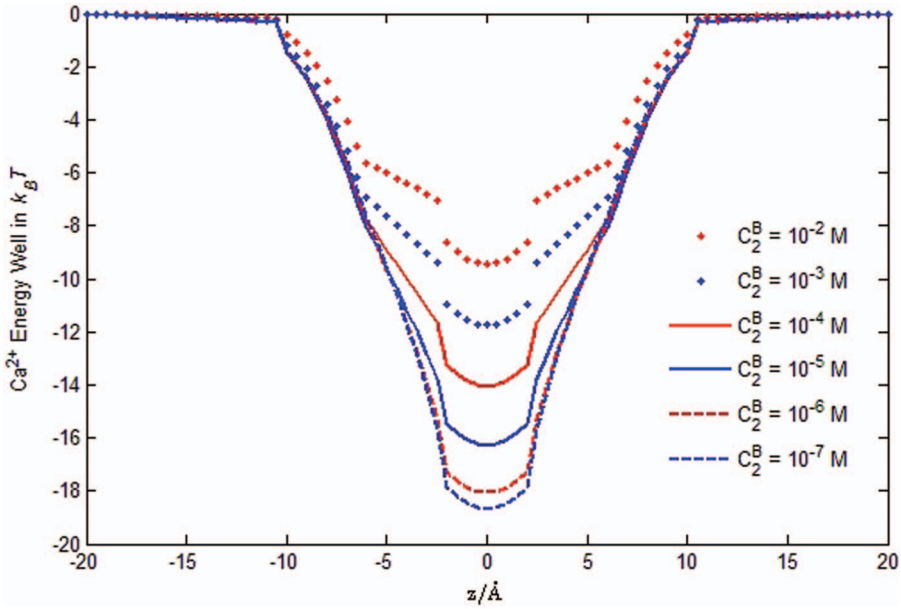

FIG. 8. Ionic energy wells. The averaged Ca^{2+} energy wells $\mathcal{E}_2(\mathbf{r}) = \beta_2\phi(\mathbf{r}) - S^{\text{trc}}(\mathbf{r})$ show the importance of the steric energy function $S^{\text{trc}}(\mathbf{r})$. Our analysis is the first to include a steric energy function, as far as we know.

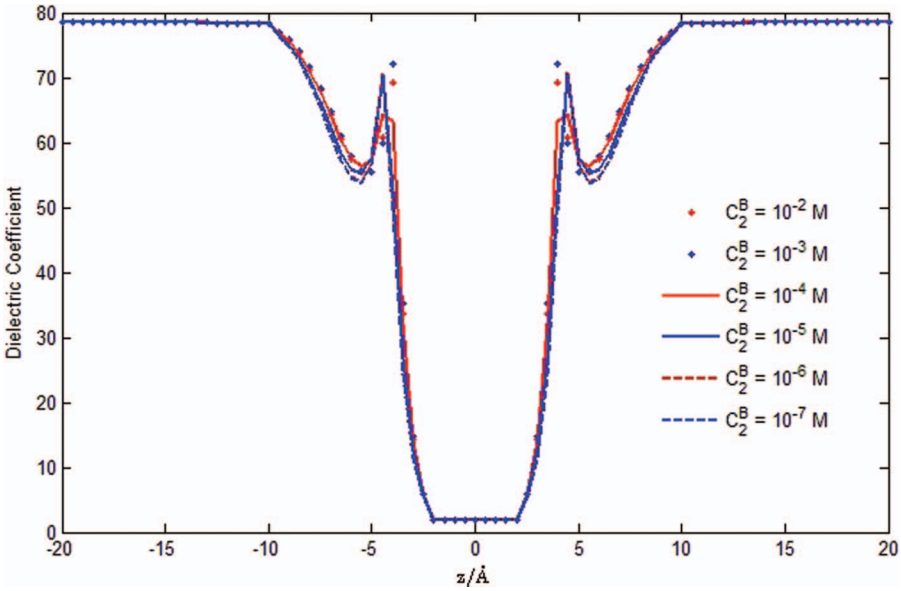

FIG. 9. Dielectric function. The averaged dielectric coefficient $\widetilde{\varepsilon}(\mathbf{r})$ profiles represent the combined effects of the dielectric response of protein atoms, the screening effect of water molecules, and the correlation effect of crowded ions. Our analysis is the first to compute the dielectric function as an output, as far as we know. Few if any other analyses include the screening effects of water molecules, the correlation of crowded ions, and the dielectric properties of the channel protein.

because the ionic atmosphere in DFT-PNP does not change with gradients of potentials, or flow. The "ionic atmosphere" of a channel is not likely to vary as much as that of a bulk solution, as long as the structure and distribution of permanent charge in the channel is unchanged. Hence, DFT-PNP is more likely to be a good description of a channel than bulk solution.

A number of effects discussed at length in the classical literature of ionic conductance[78] are not included in DFT-PNP: (i) electrophoretic and (ii) relaxation components of conductance; (iii) the spatial variation in dielectric coefficient;[15] (iv) dielectric friction;[80,81] and (v) dielectrophoresis.[82] In channels, dielectrophoresis is likely to be the most important of these five neglected effects because it depends on the second (spatial) derivative of potential. The complex charge distributions in and near ion channels are likely to produce large second derivatives of potential[83] as shown in Fig. 9. These effects arise automatically (with little need for physical discussion) in a mathematically consistent treatment of flow based on variational principles[6,11,29–31] and the Poisson-Fermi theory.[15]

Zhang *et al.*[84] have proposed a simple 1D model of all-spheres in a cylindrical channel. Their primary parameters for investigation were channel length, the concentration of protein charges (called "doping" in their papers), and salt concentrations. They show that the barrier energies decrease when the doping charge increases. We show a related phenomenon here. Barrier energies—the energy wells in Fig. 8—decrease when the Ca^{2+} bath concentration increases. Another important feature of their work is the phase transitions seen under some conditions—e.g., for long enough channels—as ions of different valence exchange places in the open channel. The exchange is equivalent to the classical blockage of the Na^+ current by increasing Ca^{2+} bath concentration discussed extensively in the literature and in our papers.

The Fermi distribution is in fact used extensively in the classical physiological literature[63] to describe two state systems that are always filled with something or other. There it is called the "Boltzmann equation" (starting we think with p. 144 of Ref. 85 and p. 503 of Ref. 86, also see Ref. 87). In particular, channologists universally use the "Boltzmann equation" to describe saturating phenomena in voltage dependence of ionic conductance, whether macroscopic or of single channels. In modern "single channel" language, this is called the voltage dependence of the number of open channels.[87–89] We hope readers from biophysics and physiology are not confused by the different usage of the term here. Our systems of (always) open channels are quite different from sometimes open, sometimes closed channels. We use "Boltzmann distribution" as it is used in statistical mechanics[26,90] to describe phenomena that do not saturate.

B. Application to a known structure

We make a final remark on how to use the simple algebraic model (4)-(7) for real protein structures. This model has been applied to study the binding mechanism of one Ca^{2+} and three Na^+ binding sites in the sodium/calcium exchanger (NCX) crystallized by Liao *et al.* in Ref. 32. Detailed analysis and results of modeling the NCX transporter will be reported elsewhere. Here, we outline our approach starting with the structure of NCX provided in the Protein Data Bank[91] (PDB ID: 3v5u) that contains 4591 atoms and four binding ions, namely, one Ca^{2+} ion and three Na^+ ions (denoted by HETATM in the PDB file) for which the occupancy numbers ranging from 0.54 to 1 are given in the file.

(1) The occupancy number is taken as the probability P_1 or P_2 for each one of the four binding sites with the specific bath condition $C^{\mathrm{B}}_{\mathrm{Na}^+}$ and $C^{\mathrm{B}}_{\mathrm{Ca}^{2+}}$ given in Ref. 32 for the PDB file.

(2) The upper limit of the summation in Eq. (6) is $N = 4591$ and the filter dielectric constant is chosen as $\epsilon_f = 30$ as an initial estimate of the combined dielectric screening effect of so many protein atoms. This is a fitting parameter that may be adjusted as analysis proceeds to fit data. Of course, only one value should be used for a whole set of experiments. The value should not be adjusted as concentrations, potentials, or compositions change.

(3) The locations $c_j, j = 1, \ldots, N$, of all protein atoms given in the PDB file are used and the corresponding atomic charges z_j are provided by the PDB2PQR software.[92] At each binding site, the binding potential ϕ_A is calculated by Eq. (6) (not by Eq. (4) or (7)) by taking the averaged value at six different points A on the surface of the binding site with fixed binding distances d_O^{Na} and d_O^{Ca} as provided by the PDB file. Changes, i.e., flexibility, in the structure, as bath concentrations change is described by forces, not by locations. That is to say, changes with concentration and so on are the result of the steric energy computed (as an output) by our model, not by explicit changes in the location, at least in this first iteration of our approach.

(4) We must deal with conditions in which occupancy numbers are not available from the PDB file. We think it is most robust to initially assume that the four different values of ϕ_A from Eq. (6) at the four binding sites are fixed when the bath conditions C_1^{B} and C_2^{B} in (7) are varied to obtain different probabilities P_1 and P_2. Of course, in later iterations of our approach this initial assumption may be improved.

IV. CONCLUSION

A molecular-continuum model of the Poisson-Fermi theory is proposed to study the binding mechanism in a L-type calcium channel. Using the explicit molecular data of the binding ion and the oxygen ions in the glutamate side chains of the channel protein, we present analytical formulas for constructing the potential and concentration functions that connect the experimental data measured in the bath to the very far away binding site. The flexibility of the glutamate side chains and the Na^+ and Ca^{2+} binding curves obtained by the proposed Fermi-like distribution over a 10^6-fold range of Ca^{2+} concentrations have been shown to agree with those of molecular dynamics or Monte Carlo. The potential, concentration, and dielectric coefficient profiles from the bath to the binding site were then obtained as outputs of the algebraic analysis and the numerical solution of the Poisson-Fermi differential equation that includes correlation and steric effects of all ions and water molecules with different sizes and valences in the channel system. Our analysis seems to be the first that includes voids and water molecules, albeit crudely. This and our earlier work is the first to apply a Fermi distribution to issues of permeation and selectivity in calcium channels, as far as we know. Taking into account the effects of the excluded volumes of the atoms of the protein, mobile ions, and water molecules with interstitial voids between particles, the steric energy improves the classical rate theory in describing the energy landscape of ions in the channel. The flexibility of protein structures is described by the steric energy which is an output of our model. The electrostatic potential of the model seems to be the evolutionary phenotype, responsible for the main physical property of the channel, the binding of calcium ions. Some guidelines of using the algebraic formulas proposed in this paper for modeling real protein structures are also briefly addressed.

ACKNOWLEDGMENTS

This work was support in part by National Science Council of Taiwan (NSCT) under Grant No. 102-2115-M-134-005 to J.L.L. and by the Bard Endowed Chair of Rush University Medical Center, held by B.E.

[1] W. Nonner and B. Eisenberg, Biophys. J. **75**, 1287 (1998).
[2] W. Nonner, L. Catacuzzeno, and B. Eisenberg, Biophys. J. **79**, 1976 (2000).
[3] W. Nonner, D. Gillespie, D. Henderson, and B. Eisenberg, J. Phys. Chem. B **105**, 6427 (2001).
[4] B. Eisenberg, Biophys. Chem. **100**, 507 (2003).
[5] B. Eisenberg, in *Advances in Chemical Physics*, edited by S. A. Rice (John Wiley and Sons, 2011), p. 77.
[6] B. Eisenberg, Y. Hyon, and C. Liu, J. Chem. Phys. **133**, 104104 (2010).
[7] J. Giri, J. E. Fonseca, D. Boda, D. Henderson, and B. Eisenberg, Phys. Biol. **8**, 026004 (2011).
[8] Y. K. Hyon, B. Eisenberg, and C. Liu, Commun. Math. Sci. **9**, 459 (2011).
[9] E. Csanyi, D. Boda, D. Gillespie, and T. Kristof, Biochim. Biophys. Acta **1818**, 592 (2012).
[10] Z. Hato, D. Boda, and T. Kristof, J. Chem. Phys. **137**, 054109 (2012).
[11] T.-L. Horng, T.-C. Lin, C. Liu, and B. Eisenberg, J. Phys. Chem. B **116**, 11422 (2012).
[12] B. Eisenberg, Biophys. J. **104**, 1849 (2013).
[13] D. Boda, D. Henderson, and D. Gillespie, J. Chem. Phys. **139**, 055103 (2013).
[14] B. Eisenberg, T.-L. Horng, T.-C. Lin, and C. Liu, Biophys. J. **104**, 509a (2013).
[15] J.-L. Liu and B. Eisenberg, J. Phys. Chem. B **117**, 12051 (2013).
[16] T. C. Lin and B. Eisenberg, Commun. Math. Sci. **12**, 149 (2014).
[17] H. Miedema, M. Vrouenraets, J. Wierenga, D. Gillespie, B. Eisenberg, W. Meijberg, and W. Nonner, Biophys. J. **91**, 4392 (2006).
[18] M. Vrouenraets, J. Wierenga, W. Meijberg, and H. Miedema, Biophys. J. **90**, 1202 (2006).
[19] H. Miedema, M. Vrouenraets, J. Wierenga, W. Meijberg, G. Robillard, and B. Eisenberg, Nano Lett. **7**, 2886 (2007).
[20] D. Boda, W. Nonner, M. Valiskó, D. Henderson, B. Eisenberg, and D. Gillespie, Biophys. J. **93**, 1960 (2007).
[21] A. Malasics, D. Gillespie, W. Nonner, D. Henderson, B. Eisenberg, and D. Boda, Biochim. Biophys. Acta **1788**, 2471 (2009).
[22] E. H. Lieband and B. Simon, Adv. Math. **23**, 22 (1977).
[23] A. A. Kornyshev, J. Phys. Chem. B **111**, 5545 (2007).
[24] M. Z. Bazant, M. S. Kilic, B. D. Storey, and A. Ajdari, Adv. Colloid Interface Sci. **152**, 48 (2009).
[25] J.-L. Liu, J. Comput. Phys. **247**, 88 (2013).
[26] D. A. McQuarrie, *Statistical Mechanics* (Harper and Row, New York, 1976).
[27] G. D. Mahan, *Many-Particle Physics* (Plenum, New York, 1993).
[28] D. Jimenez-Morales, J. Liang, and B. Eisenberg, Eur. Biophys. J. **41**, 449 (2012).
[29] Y. Mori, C. Liu, and R. S. Eisenberg, Physica D **240**, 1835 (2011).
[30] G.-W. Wei, Q. Zheng, Z. Chen, and K. Xia, SIAM Rev. **54**, 699 (2012).
[31] Y. Qiao, B. Tu, and B. Lu, J. Chem. Phys. **140**, 174102 (2014).
[32] J. Liao, H. Li, W. Zeng, D. B. Sauer, R. Belmares, and Y. Jiang, Science **335**, 686 (2012).
[33] W. Almers and E. W. McCleskey, J. Physiol. **353**, 585 (1984).
[34] D. D. Friel and R. W. Tsien, Proc. Natl. Acad. Sci. U.S.A. **86**, 5207 (1989).
[35] W. Nonner, D. P. Chen, and B. Eisenberg, Biophys. J. **74**, 2327 (1998).
[36] A. Rodriguez-Contreras, W. Nonner, and E. N. Yamoah, J. Physiol. **538**, 729 (2002).
[37] D. Gillespie and D. Boda, Biophys. J. **95**, 2658 (2008).
[38] D. Gillespie, J. Giri, and M. Fill, Biophys. J. **97**, 2212 (2009).

[39]T. Tanabe, H. Takeshima, A. Mikami, V. Flockerzi, H. Takahashi, K. Kangawa, M. Kojima, H. Matsuo, T. Hirose, and S. Numa, Nature (London) **328**, 313 (1987).
[40]S. H. Heinemann, H. Terlau, W. Stuhmer, K. Imoto, and S. Numa, Nature (London) **356**, 441 (1992).
[41]J. Yang, P. T. Ellinor, W. A. Sather, J. F. Zhang, and R. W. Tsien, Nature (London) **366**, 158 (1993).
[42]S. Tang, G. Mikala, A. Bahinski, A. Yatani, G. Varadi, and A. Schwartz, J. Biol. Chem. **268**, 13026 (1993).
[43]M. S. Kim, T. Morii, L. X. Sun, K. Imoto, and Y. Mori, FEBS Lett. **318**, 145 (1993).
[44]G. Mikala, A. Bahinski, A. Yatani, S. Tang, and A. Schwartz, FEBS Lett. **335**, 265 (1993).
[45]W. A. Sather, J. Yang, and R. W. Tsien, Curr. Opin. Neurobiol. **4**, 313 (1994).
[46]A. Yatani, A. Bahinski, G. Mikala, S. Yamamoto, and A. Schwartz, Circ. Res. **75**, 315 (1994).
[47]P. T. Ellinor, J. Yang, W. A. Sather, J. F. Zhang, and R. W. Tsien, Neuron **15**, 1121 (1995).
[48]A. Bahinski, A. Yatani, G. Mikala, S. Tang, S. Yamamoto, and A. Schwartz, Mol. Cell. Biochem. **166**, 125 (1997).
[49]S. M. Cibulsky and W. A. Sather, J. Gen. Physiol. **116**, 349 (2000).
[50]G. M. Lipkind and H. A. Fozzard, Biochemistry **40**, 6786 (2001).
[51]G. Barreiro, C. R. Guimaraes, and R. B. de Alencastro, Protein Eng. **15**, 109 (2002).
[52]X. H. Chen, I. Bezprozvanny, and R. W. Tsien, J. Gen. Physiol. **108**, 363 (1996).
[53]U. Klockner, G. Mikala, A. Schwartz, and G. Varadi, J. Biol. Chem. **271**, 22293 (1996).
[54]X. H. Chen and R. W. Tsien, J. Biol. Chem. **272**, 30002 (1997).
[55]X. S. Wu, H. D. Edwards, and W. A. Sather, J. Biol. Chem. **275**, 31778 (2000).
[56]X. Wang, T. A. Ponoran, R. L. Rasmusson, D. S. Ragsdale, and B. Z. Peterson, Biophys. J. **89**, 1731 (2005).
[57]B. Eisenberg, J. Phys. Chem. C **114**, 20719 (2010).
[58]V. Vlachy, Annu. Rev. Phys. Chem. **50**, 145 (1999).
[59]R. R. Netz and H. Orland, Eur. Phys. J. E **1**, 203 (2000).
[60]P. Grochowski and J. Trylska, Biopolymers **89**, 93 (2008).
[61]B. Eisenberg, SIAM News **45**, 11–12 (2012).
[62]W. A. Sather and E. W. McCleskey, Annu. Rev. Physiol. **65**, 133 (2003).
[63]B. Hille, *Ionic Channels of Excitable Membranes* (Sinauer Associates, Inc., Sunderland, MA, 2001).
[64]E. R. Cohen, T. Cvitas, J. Frey, B. Holmstrom, K. Kuchitsu, R. Marquardt, I. Mills, F. Pavese, M. Quack, J. Stohner, H. L. Strauss, M. Takami, and A. J. Thor, *Quantities, Units and Symbols in Physical Chemistry* (Royal Society of Chemistry Publishing, Cambridge, UK, 2007).
[65]R. S. Eisenberg, J. Membr. Biol. **115**, 1 (1990).
[66]C. D. Santangelo, Phys. Rev. E **73**, 041512 (2006).
[67]M. Z. Bazant, B. D. Storey, and A. A. Kornyshev, Phys. Rev. Lett. **106**, 046102 (2011).
[68]W. Geng, S. Yu, and G. Wei, J. Chem. Phys. **127**, 114106 (2007).
[69]D. Gillespie, W. Nonner, and R. S. Eisenberg, J. Phys. Condens. Matter **14**, 12129 (2002).
[70]D. Gillespie, Biophys. J. **94**, 1169 (2008).
[71]Y. Rosenfeld, M. Schmidt, H. Loewen, and P. Tarazona, Phys. Rev. E **55**, 4245 (1997).
[72]R. Eisenberg and D. Chen, Biophys. J. **64**, A22 (1993).
[73]M. Z. Bazant, K. Thornton, and A. Ajdari, Phys. Rev. E **70**, 021506 (2004).
[74]B. Eisenberg, Trans. Faraday Soc. **160**, 279 (2013).
[75]R. S. Eisenberg in *New Developments and Theoretical Studies of Proteins*, edited by R. Elber (World Scientific, Philadelphia, 1996), p. 269.
[76]R. D. Coalson and M. G. Kurnikova, IEEE Trans. Nanobiol. **4**, 81 (2005).
[77]R. M. Fuoss and L. Onsager, J. Phys. Chem. **62**, 1339 (1958).
[78]J.-C. Justice, in *Comprehensive Treatise of Electrochemistry. Volume 5: Thermodynamic and Transport Properties of Aqueous and Molten Electrolytes*, edited by B. E. Conway, J. O. M. Bockris, and E. Yaeger (Plenum, New York, 1983), p. 223.
[79]K. J. Laidler, J. H. Meiser, and B. C. Sanctuary, *Physical Chemistry* (Brooks Cole, Belmont, CA, 2003).
[80]J. Hubbard and L. Onsager, J. Chem. Phys. **67**, 4850 (1977).
[81]R. P. Matthews, G. A. Venter, and K. J. Naidoo, J. Phys. Chem. B **115**, 1045 (2011).
[82]H. A. Pohl, *Dielectrophoresis: The Behavior of Neutral Matter in Nonuniform Electric Fields* (Cambridge University Press, New York, 1978).
[83]R. S. Eisenberg, J. Membr. Biol. **150**, 1 (1996).
[84]J. Zhang, A. Kamenev, and B. I. Shklovskii, Phys. Rev. Lett. **95**, 148101 (2005).
[85]A. L. Hodgkin, A. F. Huxley, and B. Katz, Arch. Sci. Physiol. **3**, 129 (1949).
[86]A. L. Hodgkin and A. F. Huxley, J. Physiol. **117**, 500 (1952).
[87]A. F. Huxley, Trends Neurosci. **25**, 553 (2002).
[88]F. J. Sigworth, Q. Rev. Biophys. **27**, 1 (1994).
[89]E. Neher in *Nobel Lectures, Physiology or Medicine 1991-1995*, edited by N. Ringertz (World Scientific, Singapore, 1997), p. 10.
[90]J. Lebowitz, Phys. Today **46**(9), 32 (1993).
[91]H. M. Berman *et al.*, Acta Crystallogr. D **58**, 899–907 (2002).
[92]T. J. Dolinsky, P. Czodrowski, H. Li, J. E. Nielsen, J. H. Jensen, G. Klebe, and N. A. Baker, Nucleic Acids Res. **35**, W522–W525 (2007).